10658 *Inorg. Chem.* **2009**, *48*, 10658–10669
DOI: 10.1021/ic901352p

Inorganic Chemistry
Article

Monofluoride Bridged, Binuclear Metallacycles of First Row Transition Metals Supported by Third Generation Bis(1-pyrazolyl)methane Ligands: Unusual Magnetic Properties

Daniel L. Reger,* Elizabeth A. Foley, Russell P. Watson, Perry J. Pellechia, and Mark D. Smith

Department of Chemistry and Biochemistry, University of South Carolina, Columbia, South Carolina, 29208

Fernande Grandjean

Department of Physics, B5, University of Liège, B-4000 Sart-Tilman, Belgium

Gary J. Long*

Department of Chemistry, Missouri University of Science and Technology,University of Missouri, Rolla, Missouri 65409-0010

Received July 11, 2009

The reaction of $M(BF_4)_2 \cdot xH_2O$, where M is Fe, Co, Cu, and Zn, and the ditopic, bis(pyrazolyl)methane ligand *m*-$[CH(pz)_2]_2C_6H_4$, $\mathbf{L_m}$, where pz is a pyrazolyl ring, yields the monofluoride bridged, binuclear $[M_2(\mu\text{-F})(\mu\text{-}\mathbf{L_m})_2](BF_4)_3$ complexes. In contrast, a similar reaction of $\mathbf{L_m}$ with $Ni(BF_4)_2 \cdot 6H_2O$ yields dibridged $[Ni_2(\mu\text{-F})_2(\mu\text{-}\mathbf{L_m})_2](BF_4)_2$. The solid state structures of seven $[M_2(\mu\text{-F})(\mu\text{-}\mathbf{L_m})_2](BF_4)_3$ complexes show that the divalent metal ion is in a five-coordinate, trigonal bipyramidal, coordination environment with either a linear or nearly linear M−F−M bridging arrangement. NMR results indicate that $[Zn_2(\mu\text{-F})(\mu\text{-}\mathbf{L_m})_2](BF_4)_3$ retains its dimeric structure in solution. The $[Ni_2(\mu\text{-F})_2(\mu\text{-}\mathbf{L_m})_2](BF_4)_2$ complex has a dibridging fluoride structure that has a six-coordination environment about each nickel(II) ion. In the solid state, the $[Fe_2(\mu\text{-F})(\mu\text{-}\mathbf{L_m})_2](BF_4)_3$ and $[Co_2(\mu\text{-F})(\mu\text{-}\mathbf{L_m})_2](BF_4)_3$ complexes show weak intramolecular antiferromagnetic exchange coupling between the two metal(II) ions with J values of −10.4 and −0.67 cm^{-1}, respectively; there is no observed long-range magnetic order. Three different solvates of $[Cu_2(\mu\text{-F})(\mu\text{-}\mathbf{L_m})_2](BF_4)_3$ are diamagnetic between 5 and 400 K, thus showing strong antiferromagnetic exchange interactions of −600 cm^{-1} or more negative. Mössbauer spectra indicate that $[Fe_2(\mu\text{-F})(\mu\text{-}\mathbf{L_m})_2](BF_4)_3$ exhibits no long-range magnetic order between 4.2 and 295 K and isomer shifts that are consistent with the presence of five-coordinate, high-spin iron(II).

Introduction

The preparation of new ligands designed to control the organization of metal complexes at both the molecular and supramolecular level has potential applications in materials design.[1] Much of our research[2] in this area is derived from the poly(pyrazolyl)methane family of scorpionate ligands that was first introduced in 1970 by Trofimenko.[3] After synthesizing a series of "second generation" tris(pyrazolyl)methane ligands, ligands with bulky groups substituted near the metal coordination site of the pyrazolyl nitrogen donor,[4] we have extended our ligand syntheses to the preparations of a series of "third generation" poly(pyrazolyl)methane ligands, ligands specifically functionalized at the non-coordinating "back" position. A major class of these third generation ligands

*To whom correspondence should be addressed. reger@mail.chem.sc.edu (D.L.R.), glong@mst.edu (G.J.L.).

(1) (a) Braga, D.; Brammer, L.; Champness, N. R. *CrystEngComm* **2005**, *7*, 1. (b) Brammer, L. *Chem. Soc. Rev.* **2004**, *33*, 476. (c) James, S. *Chem. Soc. Rev.* **2003**, *32*, 276. (d) Janiak, C. *J. Chem. Soc., Dalton Trans.* **2003**, 2781. (e) Sharma, C. V. K. *Cryst. Growth Des.* **2002**, *2*, 465.

(2) (a) Reger, D. L.; Elgin, J. D.; Semeniuc, R. F.; Pellechia, P. J.; Smith, M. D. *Chem. Commun.* **2005**, 4068. (b) Reger, D. L.; Semeniuc, R. F.; Rassolov, V.; Smith, M. D. *Inorg. Chem.* **2004**, *43*, 537. (c) Reger, D. L.; Semeniuc, R. F.; Smith, M. D. *Inorg. Chem.* **2003**, *42*, 8137. (d) Reger, D. L.; Semeniuc, R. F.; Rassolov, V.; Smith, M. D. *J. Organomet. Chem.* **2003**, *666*, 87. (e) Reger, D. L.; Gardinier, J. R.; Semeniuc, R. F.; Smith, M. D. *J. Chem. Soc., Dalton Trans.* **2003**, 1712. (f) Reger, D. L.; Wright, T. D.; Semeniuc, R. F.; Grattan, T. C.; Smith, M. D. *Inorg. Chem.* **2001**, *40*, 6212. (g) Reger, D. L.; Semeniuc, R. F.; Smith, M. D. *Inorg. Chem.* **2001**, *40*, 6545.

(3) Trofimenko, S. *J. Am. Chem. Soc.* **1970**, *92*, 5118.

(4) Reger, D. L.; Grattan, T. C.; Brown, K. J.; Little, C. A.; Lamba, J. J. S.; Rheingold, A. L.; Sommer, R. D. *J. Organomet. Chem.* **2000**, *607*, 120.

 Published on Web 10/14/2009

Chart 1. Drawing of *m*-$[CH(pz)_2]_2C_6H_4$, $\mathbf{L}_m$

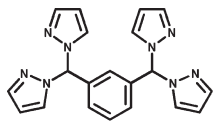

$\mathbf{L}_m$

contains multiple poly(pyrazolyl)methane units linked in a single molecule.[2,5] By controlling the directional orientation of the poly(pyrazolyl)methane units with a fixed central organic core, by altering the flexibility of the group linking this core with the poly(pyrazolyl)methane donor units, and by using both bis- and tris(pyrazolyl)methane donor units, it is possible to control the molecular, and to a lesser extent, the supramolecular structures of metal complexes.[2,5] Analogous ditopic bis(pyrazolyl)borate and related ligands have also been investigated.[6]

The chemistry of the ditopic *m*-$[CH(pz)_2]_2C_6H_4$, $\mathbf{L}_m$ in Chart 1, ligand where pz is a pyrazolyl ring, is particularly interesting because the *meta*-orientation of two bis(pyrazolyl)methane units directly fused to an aromatic ring leads to the formation of binuclear metallacyclic complexes. Our initial work dealt with the syntheses of silver(I) complexes, such as $[Ag_2(\mu\text{-}\mathbf{L}_m)_2](PF_6)_2$, see Figure 1a, where we demonstrated that $\mathbf{L}_m$ supported the formation of binuclear metallacycles and, more importantly, were flexible enough to support Ag···Ag nonbonding distances that varied from 4.10 to 5.31 Å.[5b] We then demonstrated that the higher charged iron(II), zinc(II), and cadmium(II) ions in addition to forming the binuclear metallacycles promoted fluoride abstraction from a BF_4^- anion to produce $[Fe_2(\mu\text{-}F)(\mu\text{-}\mathbf{L}_m)_2](BF_4)_3$ and $[Zn_2(\mu\text{-}F)(\mu\text{-}\mathbf{L}_m)_2](BF_4)_3$,[5c] complexes that have unusual linear or nearly linear M−F−M bridging units,[7] see Figure 1b, and $[Cd_2(\mu\text{-}F)_2(\mu\text{-}\mathbf{L}_m)_2](BF_4)_2$.[5c]

Because of the potential for unusual physical properties of the linear M−F−M bridged complexes, we extended the series of first row divalent transition metal complexes to include the metals between iron and zinc and have examined the whole series with an emphasis on solid-state magnetic properties. We anticipated that the linear M−F−M fluoride bridge might yield strong intramolecular antiferromagnetic exchange interactions[8] and were, thus, particularly interested in determining how the exchange interactions would vary with the number of 3d metal electrons in this homologous series of complexes. The resulting synthesis, crystal structures, and magnetic properties are reported herein along with a Mössbauer spectral study of $[Fe_2(\mu\text{-}F)(\mu\text{-}\mathbf{L}_m)_2](BF_4)_3$.

Experimental Section

General Considerations. Air sensitive materials were handled under a nitrogen atmosphere using standard Schlenk techniques or in a Vacuum Atmospheres HE-493 drybox. All solvents were dried by conventional methods prior to use. The *m*-$[CH(pz)_2]_2C_6H_4$[5b] ligand and $[M_2(\mu\text{-}F)(\mu\text{-}m\text{-}[CH(pz)_2]_2C_6H_4)_2](BF_4)_3$ (M = Fe (**1**), Zn (**5**))[5c] complexes were prepared following reported procedures. All other chemicals were purchased from Aldrich or Fisher Scientific and used as received. Reported melting points are uncorrected.

^1H, ^{13}C, and ^{19}F NMR spectra were recorded on a Varian Mercury/VX 300, Varian Mercury/VX 400, or Varian INOVA 500 spectrometer. Solid-State NMR spectra were recorded on a Varian INOVA 500 spectrometer. All chemical shifts are in ppm and were referenced to residual undeuterated solvent signals (^1H), deuterated solvent signals (^{13}C), or externally to $CFCl_3$ (^{19}F). Mass spectrometric measurements were obtained on a MicroMass QTOF spectrometer in an acid-free environment. Reflectance spectra were recorded on a Perkin-Elmer Lambda 35 UV/vis spectrometer with a white tile used as reference for 100% reflectance. Solution UV−vis measurements were recorded on a Hewlett-Packard 8453 UV−vis spectrometer. Elemental analyses were performed on vacuum-dried samples by Robertson Microlit Laboratories (Madison, NJ). Solution magnetic susceptibilities were determined at 295 K by the Evans method.[9] The thermogravimetric analysis was run on a TA Instruments SDT 2960 simultaneous TGA·DTA at a rate of 10 °C/min.

The magnetic properties were measured in the solid state with a Quantum Design MPMSXL superconducting quantum interference magnetometer. Gelatin capsules designed to prevent sample movement were used as sample containers that make a negligible contribution to the overall magnetization. Complex **1** was zero-field cooled to 2 K and warmed and cooled between 2 and 300 K in an applied field of 1.0 T, whereas the other complexes were zero-field cooled to 5 K and warmed and cooled between 5 and 300 K in an applied field of 0.7 T. Complex $\mathbf{4}\cdot 0.71H_2O$ was also studied from 200 to 400 K in an applied field of 0.7 T. In each case there was no significant difference between the moments obtained upon warming and cooling, and the moments have been merged. Diamagnetic corrections of −0.000487, −0.000601, −0.000498, and −0.000605 emu/mol of dimer, obtained from tables of Pascal's constants, have been applied to the measured susceptibility of the Fe, Co, Ni, and Cu complexes, respectively. The details of the fitting procedures used to understand the magnetic properties of each of the complexes are given in the Supporting Information.

The Mössbauer spectra of **1** have been measured between 4.2 and 295 K on a constant-acceleration spectrometer that utilized a 295 K rhodium matrix cobalt-57 source and was calibrated at 295 K with α-iron powder. The spectra have been measured on an absorber that contained 50 mg/cm^2 of sample that had been crushed but not ground and dispersed in boron nitride powder. The observed spectra have been fit with one symmetric quadrupole doublet, and the estimated relative errors are ± 0.005 mm/s for the isomer shifts, ± 0.01 mm/s for the quadrupole splittings and line widths, and ± 0.005 (%ε)(mm/s) for the spectral

(5) (a) Reger, D. L.; Foley, E. A.; Semeniuc, R. F.; Smith, M. D. *Inorg. Chem.* **2007**, *46*, 11345. (b) Reger, D. L.; Watson, R. P.; Smith, M. D. *Inorg. Chem.* **2006**, *45*, 10077. (c) Reger, D. L.; Watson, R. P.; Gardinier, J. R.; Smith, M. D.; Pellechia, P. J. *Inorg. Chem.* **2006**, *45*, 10088. (d) Reger, D. L.; Watson, R. P.; Gardinier, J. R.; Smith, M. D. *Inorg. Chem.* **2004**, *43*, 6609. (e) Reger, D. L; Foley, E. A.; Smith, M. D. *Inorg. Chem.* **2009**, *48*, 936.

(6) Zhang, F.; Morawitz, T.; Bieller, S.; Bolte, M.; Lerner, H.-W.; Wagner, M. *J. Chem. Soc., Dalton Trans.* **2007**, 4594, and references therein.

(7) (a) Leo, R.; Massa, W.; Pebler, J. *J. Fluorine Chem.* **2004**, *125*, 923. (b) Westerheide, L.; Müller, F. K.; Than, R.; Krebs, B.; Dietrich, J.; Schindler, S. *Inorg. Chem.* **2001**, *40*, 1951. (c) Choudhury, A.; Rao, C. N. R. *J. Struct. Chem.* **2002**, *43*, 632. (d) Hao, H.; Cui, C.; Herbert, W.; Bai, G.; Schmidt, H.-G.; Noltemeyer, M. *Chem. Commun.* **2001**, 1118. (e) Yu, P.; Muller, P.; Roesky, H. W.; Noltemeyer, M.; Demsar, A.; Uson, I. *Angew. Chem., Int. Ed.* **1999**, *38*, 3319. (f) Mrak, M.; Helliwell, M.; Ristic, A.; Logar, N. Z.; Kaucic, V. *Acta Chim. Slov.* **2001**, *48*, 147. (g) Wang, C.-M.; Liao, C.-H.; Kao, H.-M.; Lii, K.-H. *Inorg. Chem.* **2005**, *44*, 6294. (h) Worm, K.; Chu, F.; Matsumoto, K.; Best, M. D.; Lynch, V.; Anslyn, E. V. *Chem.—Eur. J.* **2003**, *9*, 741. (i) Vela, J.; Smith, J. M.; Yu, Y.; Ketterer, N. A.; Flaschenreim, C. J.; Lachicotte, R. J.; Holland, P. L. *J. Am. Chem. Soc.* **2005**, *127*, 7857. (j) Tomat, E.; Cuesta, L.; Lynch, V. M.; Sessler, J. L. *Inorg. Chem.* **2007**, *46*, 6224.

(8) Kahn, O. *Molecular Magnetism*; VCH Publishers, Inc.: New York, 1993.

(9) (a) Sur, S. K. *J. Magn. Reson.* **1989**, *82*, 169. (b) Evans, D. F. *J. Chem. Soc.* **1959**, 2003.

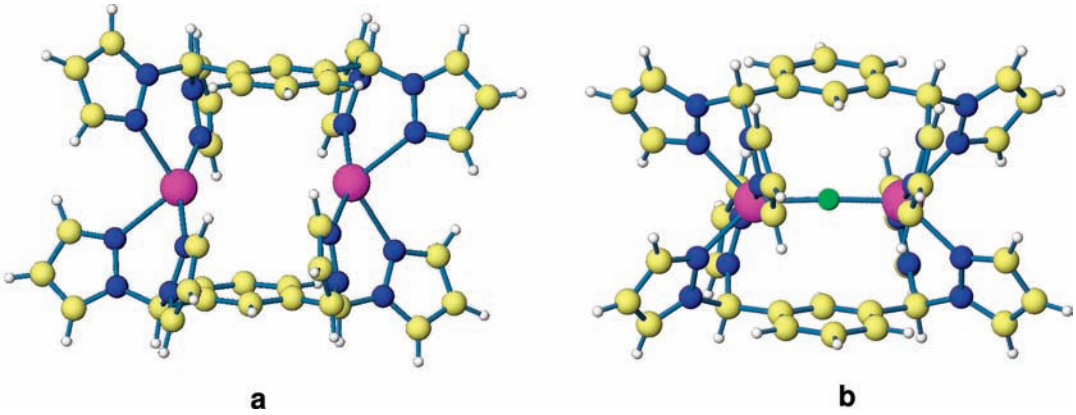

Figure 1. (a) $[Ag_2(\mu\text{-}\mathbf{L}_m)_2]^{2+}$, (b) $[M_2(\mu\text{-F})(\mu\text{-}\mathbf{L}_m)_2]^{3+}$ with M = Fe and Zn.

absorption areas. The absolute errors are approximately twice as large.

$[Co_2(\mu\text{-F})(\mu\text{-}m\text{-}[CH(pz)_2]_2C_6H_4)_2](BF_4)_3$, 2. A rose-colored, 10 mL tetrahydrofuran (THF) solution of $Co(BF_4)_2 \cdot 6H_2O$ (0.46 g, 1.4 mmol) was added by cannula to a 15 mL THF solution of m-$[CH(pz)_2]_2C_6H_4$ (0.50 g, 1.3 mmol). A pink precipitate immediately formed, and the system was stirred at room temperature for 2 d. The solid was isolated by cannula filtration, washed with 10 mL of THF, and dried in vacuo overnight, affording 0.76 g (99%) of the crude product. Single crystals suitable for X-ray studies were grown by the vapor diffusion of Et_2O into 1 mL acetone solutions of **2** and were mounted directly from the mother liquor. Crystals used for elemental analysis were removed from the mother liquor, rinsed with ether, and dried in vacuo, which resulted in loss of solvent of crystallization. Mp >300 °C. Anal. Calcd.(Found) for $C_{40}H_{36}B_3Co_2F_{13}N_{16}$: C, 42.21 (41.97); H, 3.19 (2.91); N, 19.69 (19.39). ^{1}H NMR (400 MHz, CD_3CN): δ 79.69 (s), 64.71 (s), 59.88 (s), 44.65 (s), 41.28 (s), 33.03 (s), 30.19 (s), 29.83 (s), 23.76 (s), 16.04 (s), 6.22 (s), −30.17 (s). ^{19}F NMR (376 MHz, CD_3CN): δ −150 (BF_4^-). Solution μ_{eff} per dimer (400 MHz, CD_3CN) 4.82 μ_B. MS ESI(+) m/z (rel. % abund.) [assgn]: 983 (11) $[Co_2(\mathbf{L}_m)_2F_2(BF_4)]^+$, 915 (4) $[Co_2(\mathbf{L}_m)_2F_3]^+$, 886 (57) $[Co(\mathbf{L}_m)_2BF_4]^+$, 818 (100) $[Co(\mathbf{L}_m)_2F]^+$, 448 (37) $[Co(\mathbf{L}_m)F]^+$, 371 (33) $[\mathbf{L}_m + H]^+$, 292 (8) $[Co_2(\mathbf{L}_m)_2F]^{3+}$. HRMS: ES$^+$ (m/z): $[Co_2(\mathbf{L}_m)_2F_3]^+$ calcd for $[C_{40}H_{36}Co_2F_3N_{16}]^+$ 915.1925; found 915.1885. UV−vis (CH_3CN), λ_{max} (ε/M^{-1} cm^{-1}): 272 (3.6×10^3), 295 (2.7×10^3), 502 (2.9×10^1).

$[Ni_2(\mu\text{-F})_2(\mu\text{-}m\text{-}[CH(pz)_2]_2C_6H_4)_2](BF_4)_2$, 3. A blue-green colored, 10 mL THF solution of $Ni(BF_4)_2 \cdot 6H_2O$ (0.19 g, 0.6 mmol) was added by cannula to a 50 mL THF solution of m-$[CH(pz)_2]_2C_6H_4$ (0.21 g, 0.6 mmol). A blue precipitate immediately formed, and the system was stirred at room temperature overnight. The solid was isolated by cannula filtration, washed with 10 mL of THF, and dried in vacuo overnight, affording 0.31 g of the crude product. Single crystals suitable for X-ray studies were grown by the vapor diffusion of Et_2O into 1 mL acetonitrile solutions of **3** and were mounted directly from the mother liquor. Samples of **3** for the magnetic data and mass spectrometry were obtained by the vapor diffusion of Et_2O into 1 mL acetonitrile solution (10 mg/mL). The mother liquor was removed, the solid in the tubes was washed with diethyl ether, and removed from the tube. The recovered material was dried in vacuo for 4 days. MS ESI(+) m/z (rel. % abund.) [assgn]: 981 (10) $[Ni_2(\mathbf{L}_m)_2F_2(BF_4)]^+$, 885 (45) $[Ni(\mathbf{L}_m)_2(BF_4)]^+$, 817 (19) $[Ni(\mathbf{L}_m)_2F]^+$, 515 (11) $[Ni_2(\mathbf{L}_m)_2(BF_4)_2]^{2+}$, 447 (94) $[Ni_2(\mathbf{L}_m)_2F_2]^{2+}$, 371 (16) $[\mathbf{L}_m + H]^+$. HRMS: ES$^+$ (m/z): $[Ni_2(\mathbf{L}_m)_2F_2(BF_4)]^+$ calcd for $[C_{40}H_{36}{}^{10}BNi_2F_6N_{16}]^+$ 980.2049; found 980.2050.

$[Cu_2(\mu\text{-F})(\mu\text{-}m\text{-}[CH(pz)_2]_2C_6H_4)_2](BF_4)_3$, 4. A 15 mL THF solution of m-$[CH(pz)_2]_2C_6H_4$ (0.50 g, 1.3 mmol) was added by cannula to a blue, 10 mL THF solution of $Cu(BF_4)_2 \cdot 3H_2O$ (0.39 g, 1.3 mmol). A blue precipitate immediately formed, and the system was stirred at room temperature overnight. The solid was isolated by cannula filtration, washed with 5 mL of THF, and dried in vacuo overnight, affording 0.62 g (81%) of the crude product. Single crystals suitable for X-ray studies were grown by the vapor diffusion of Et_2O into 1 mL acetonitrile solutions of **4** and were mounted directly from the mother liquor. Crystals used for elemental analysis were grown from acetonitrile, removed from the mother liquor, rinsed with ether, and dried in vacuo, which resulted in loss of solvent of crystallization. Dec. 210−263 °C. Anal. Calcd.(Found) for $C_{40}H_{36}B_3Cu_2F_{13}N_{16}$: C, 41.87 (41.65); H, 3.16 (3.05); N, 19.53 (19.35). ^{1}H NMR (400 MHz, CD_3CN): δ 29.70 (s), 24.55 (s), 18.61 (s), 15.34 (s), 10.49 (s), 9.79 (s), 4.81(s). ^{19}F NMR (376 MHz, CD_3CN): δ −151 (BF_4^-). Solution μ_{eff} per dimer (400 MHz, CD_3CN) 2.12 μ_B. MS ESI(+) m/z (rel. % abund.) [assgn]: 822 (1) $[Cu(\mathbf{L}_m)_2F]^+$, 452 (13) $[Cu_2(\mathbf{L}_m)_2F_2]^{2+}$, 295 (30) $[Cu_2(\mathbf{L}_m)_2F]^{3+}$. UV−vis ($CH_3CN$) λ_{max} (ε/M^{-1} cm^{-1}): 272 (2.0×10^3), 289 (2.2×10^3), 798 (9.0×10^1). UV−vis (solid) λ_{max} (%R): 485 (28).

$[Cu_2(\mu\text{-}m\text{-}[CH(pz)_2]_2C_6H_4)_2](BF_4)_2$, 6. Under N_2, a 10 mL THF solution of m-$[CH(pz)_2]_2C_6H_4$ (0.21 g, 0.58 mmol) was added by cannula to a 10 mL THF solution of $[Cu(CH_3CN)_4]BF_4$ (0.18 g, 0.58 mmol). A white precipitate formed overnight as the system was stirred at room temperature. The solid was isolated by cannula filtration and dried in vacuo overnight, affording 0.207 g (69%) of the product. Dec 261−300 °C. Anal. Calcd.(Found) for $C_{40}H_{36}B_2Cu_2F_8N_{16}$: C, 46.13 (45.78); H, 3.48 (3.23); N, 21.52 (21.23). ^{1}H NMR (400 MHz, CD_3CN): δ 7.78 (s, 2H, CH(pz)$_2$), 7.73, 7.55 (s, s; 4H, 4H; 3,5-H-pz), 7.38 (t, J = 8 Hz, 1H, C_6H_4), 6.90 (d, J = 8 Hz, 2H, C_6H_4), 6.36 (s, 4H, 4-H-pz), 6.33 (s, 1H, C_6H_4). ^{19}F NMR (376 MHz, CD_3CN): δ −152 (BF_4^-). MS ESI(+) m/z (rel. % abund.) [assgn]: 953 (1) $[Cu_2(\mathbf{L}_m)_2BF_4]^+$, 803 (3) $[Cu(\mathbf{L}_m)_2]^+$, 433 (100) $[Cu(\mathbf{L}_m)]^+$, 371 (4) $[\mathbf{L}_m + H]^+$, 303 (14) $[\mathbf{L}_m - pz]^+$. UV−vis (CH_3CN): no absorbance between 300 and 1100 nm. UV−vis (solid): flat line between 375 and 800 nm.

Crystal Structure Determinations. Crystals for the solid state structures of **2**·2.17($(CH_3)_2CO$), **3**·CH_3CN, **4**·1.5CH_3CN, and **4**·2.25($(CH_3)_2CO$) were obtained by vapor diffusion of diethyl ether into acetonitrile solutions of **3** and **4**, or acetone solutions of **2** and **4**, respectively. **4**·2(H_2O) and **4**·0.71(H_2O) were obtained by drying **4**·1.5CH_3CN under vacuum and letting the crystals sit 2 weeks or a few minutes in a screw top vial, respectively. The solid state structures of **1**·1.5CH_3CN and **5**·1.5CH_3CN have been reported.[5c] X-ray diffraction intensity data from a pink prismatic crystals of **2**·2.17($(CH_3)_2CO$), a pale blue bar-shaped crystal of **3**·CH_3CN, a pale blue platelike

(10) *SMART Version 5.625 and SAINT+ Version 6.22*; Bruker Analytical X-ray Systems, Inc.: Madison, WI, 2001.

Table 1. Selected Crystal Data and Structure Refinement

	2·2.17($(CH_3)_2CO$)	**3**·CH_3CN	**4**·2.25($(CH_3)_2CO$)	**4**·1.5CH_3CN	**4**·2(H_2O)	**4**·0.71(H_2O)
formula	$C_{46.50}H_{49}B_3Co_2F_{13}N_{16}O_{2.17}$	$C_{42}H_{39}B_2F_{10}N_{17}Ni_2$	$C_{46.75}H_{49.50}B_3Cu_2F_{13}N_{16}O_{2.25}$	$C_{43}H_{40.50}B_3Cu_2F_{13}N_{17.50}$	$C_{40}H_{40}B_3Cu_2F_{13}N_{16}O_2$	$C_{40}H_{37.41}B_3Cu_2F_{13}N_{16}O_{0.71}$
Fw, g mol^{-1}	1263.95	1110.94	1278.03	1208.94	1183.39	1160.14
cryst syst	triclinic	monoclinic	triclinic	monoclinic	monoclinic	monoclinic
space group	$P\bar{1}$	$P2_1/c$	$P\bar{1}$	$P2_1/m$	$P2_1/m$	$P2_1/m$
T, K	150(1)	150(1)	150(1)	150(1)	150(1)	150(1)
a, Å	13.3801(5)	9.1107(5)	13.3642(4)	10.1714(3)	10.4946(5)	10.2515(5)
b, Å	13.8036(5)	14.4480(8)	13.8264(4)	42.3175(14)	42.288(2)	41.947(2)
c, Å	16.5377(6)	17.0858(9)	16.4223(5)	11.8649(4)	11.3470(6)	11.6474(6)
α, deg	83.0530(10)	90	83.8870(10)	90	90	90
β, deg	76.4570(10)	93.2020(10)	76.7830(10)	103.0440(10)	102.9690(10)	104.721(1)
γ, deg	67.8010(10)	90	68.0040(10)	90	90	90
V, Å^3	2747.58(17)	2245.5(2)	2738.35(14)	4975.2(3)	4907.3(4)	4844.1(4)
Z	2	2	2	4	4	4
R1 ($I > 2\sigma(I)$)	0.0433	0.0485	0.0413	0.0428	0.0556	0.0684
wR2 ($I > 2\sigma(I)$)	0.0782	0.1102	0.0904	0.0981	0.1260	0.1540

crystal of **4**·1.5CH_3CN, a blue prismatic crystal of **4**·2.25-($(CH_3)_2CO$), a pale blue-green plate of **4**·2(H_2O), and a pale blue-green plate of **4**·0.71(H_2O) were measured at 150(1) K with Mo K_α 0.71073 Å radiation on a Bruker SMART APEX diffractometer.[10] Raw area detector data frame integration was performed with SAINT+.[10]

Final unit cell parameters were determined by least-squares refinement of large sets of strong reflections taken from each data set. Direct methods structure solution, difference Fourier calculations and full-matrix least-squares refinement against F^2 were performed with SHELXTL.[11] Most non-hydrogen atoms were refined with anisotropic displacement parameters, the exception being disordered species. Hydrogen atoms were placed in geometrically idealized positions and included as riding atoms. Details of the data collection are given in Table 1, while further details regarding the solution and refinement of the structures follow below.

The complex **2**·2.17($(CH_3)_2CO$) crystallizes in the space group $P\bar{1}$ of the triclinic system. The asymmetric unit consists of one-half of each of the two independent $[Co_2(\mu\text{-}F)(\mu\text{-}\mathbf{L}_m)_2]^{3+}$ cationic complexes, three independent BF_4^- anions, and 2.17 independent acetone molecules of crystallization; each binuclear cobalt complex resides on a crystallographic inversion center. One BF_4^- anion (B3) and $^1/_6$ of an acetone molecule are disordered together in nearby regions and were refined using geometric restraints. The $^1/_6$ acetone molecule is disordered about an inversion center. Its occupancy was derived by refinement with a fixed isotropic displacement parameter.

The complex **3**·CH_3CN crystallizes in the $P2_1/c$ space group as determined by the pattern of systematic absences in the intensity data. The asymmetric unit consists of one-half of a nickel complex $[Ni_2(\mu\text{-}F)_2(\mu\text{-}\mathbf{L}_m)_2]^{2+}$ located on a crystallographic inversion center, a BF_4^- anion disordered over two orientations, and a half-occupied acetonitrile molecule disordered across inversion center.

The complex **4**·2.25($(CH_3)_2CO$) crystallizes in the space group $P\bar{1}$ of the triclinic system. The asymmetric unit consists of half each of two independent, centrosymmetric $[Cu_2(\mu\text{-}F)(\mu\text{-}\mathbf{L}_m)_2]^{3+}$ cationic complexes, three independent BF_4^- anions, and 2.25 independent acetone molecules of crystallization. The disorder of BF_4^- anion B3 and the $^1/_4$ acetone molecule is similar to that observed in complex **2**·2.17($(CH_3)_2CO$), and was treated similarly.

The complex **4**·1.5CH_3CN crystallizes in the space group $P2_1/m$. The asymmetric unit consists of one-half of each of the two $[Cu_2(\mu\text{-}F)(\mu\text{-}\mathbf{L}_m)_2]^{3+}$ cations, three independent BF_4^- counteranions, and two acetonitrile molecules of crystallization. The copper cation Cu1 is located on an inversion center and Cu2 is located on a mirror plane. The displacement ellipsoid of the bridging fluoride atom F1 of cation Cu1 is highly elongated if refined as a single position on the inversion center. For this reason F1 was successfully modeled as split equally over two positions. Two BF_4^- ions (B2 and B3) are disordered over two closely separated orientations and were refined using geometric restraints.

The **4**·$x$$H_2O$ (x = 2 or 0.71) complexes have a similar structure, differing chiefly in the location and amount of the guest solvent molecules and in the pattern of tetrafluoroborate anion disorder. Both crystallize in the space group $P2_1/m$. In each structure the asymmetric unit consists of half each of two dicopper cations, three BF_4^- anions, and disordered water molecules. Cation Cu1 resides on an inversion center and cation Cu2 is on a mirror plane. Details pertinent to each refinement are given below.

***x* = 2.** The displacement ellipsoid of the bridging fluoride atom F1 of cation Cu1 is highly elongated (U3/U1 = 7.1) if refined as a single position on the inversion center. For this reason F1 was successfully modeled as split equally over two positions. There are two distinct water molecules, which inhabit the position occupied by one acetonitrile molecule (N91) in the acetonitrile solvated analogue; the other acetonitrile position (N92) is vacant. Each distinct water molecule is disordered equally over two closely separated sites (O1/O2 and O3/O4). Reasonable positions for the water hydrogen atoms were located in difference maps, and their coordinates adjusted to give d(O−H) near 0.84 Å. They were then refined as riding atoms with $U_{iso,H} = 1.5U_{eq,O}$. Tetrafluoroborate anion B1 is severely disordered and was modeled in three distinct orientations with manually fixed populations.

***x* = 0.71.** The F1 atom displacement ellipsoid showed only a slight elongation (U3/U1 = 3.7) and was modeled with a single position, on the inversion center. Two disordered water molecule sites O1 and O2 were identified; they occupy positions approximately midway between the O1/O2 and O3/O4 positions in the $x = 2$ crystal. These refined as partially occupied with a common displacement parameter. The refined occupancies of each site are: O1 = 0.40(2) and O2 = 0.31(1), giving the reported 0.71H_2O per formula unit. It must be noted that the occupancy and displacement parameter values are correlated such that a smaller U_{iso} value for these atoms results in a lower water content. For example, using a fixed U_{iso} value of 0.10 Å^2 gives a water content of 0.62H_2O per formula unit. Tetrafluoroborate anions B1 and B3 are both disordered, B1 with three distinct orientations and B3 with two orientations. Geometries of each disorder component were refined with geometric restraints.

Results

Syntheses of Complexes. As reported previously for the iron(II) complex **1** and zinc(II) complex **5**,[5c] the $[M_2(\mu\text{-}F)(\mu\text{-}\mathbf{L}_m)_2](BF_4)_3$ complexes with M = Co(II) (**2**) and Cu(II)

(11) Sheldrick, G. M. *SHELXTL Version 6.1*; Bruker Analytical X-ray Systems, Inc.: Madison, WI, 2000.

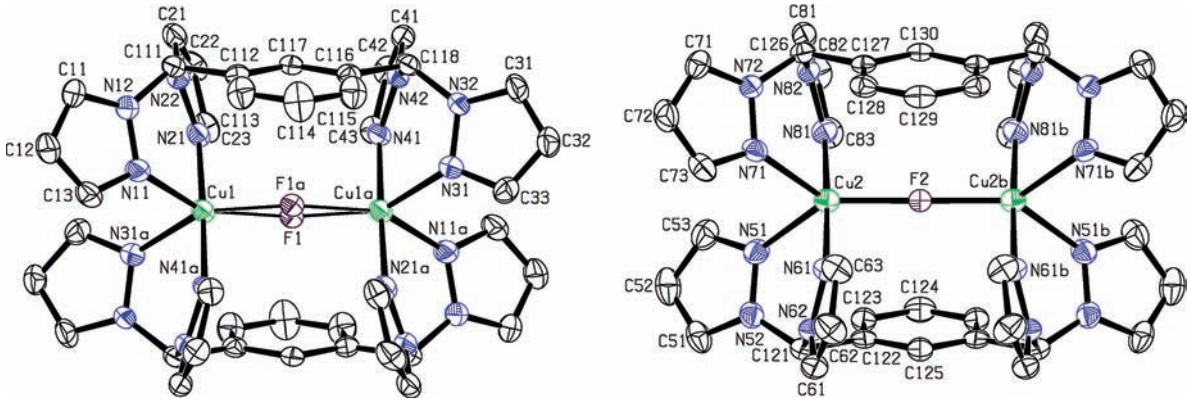

Figure 2. Structures of the two independent cations of $[Cu_2(\mu\text{-}F)(\mu\text{-}\mathbf{L}_m)_2](BF_4)_3 \cdot 1.5CH_3CN$. Hydrogen atoms omitted for clarity. The cation on the left has two half equally populated fluoride sites.

(**4**) were prepared by combining separate THF solutions of $\mathbf{L}_m$ and $M(BF_4)_2 \cdot xH_2O$ (M = Co, Cu; $x = 6, 3$) according to eq 1. Surprisingly, when the two THF solutions of $\mathbf{L}_m$ and $Ni(BF_4)_2 \cdot 6H_2O$ were combined, the difluoro-bridged complex $[Ni_2(\mu\text{-}F)_2(\mu\text{-}\mathbf{L}_m)_2](BF_4)_2$ (**3**) was isolated, as shown in eq 2. The non-fluoride bridged copper complex $[Cu_2(\mu\text{-}\mathbf{L}_m)_2](BF_4)_2$ (**6**) is formed by combining the THF solutions of $\mathbf{L}_m$ and $[Cu(CH_3CN)_4]$-BF_4, as shown in eq 3.

$$2M(BF_4)_2 + 2\mathbf{L}_m \xrightarrow{\text{solvent}} [M_2(\mu\text{-}F)(\mu\text{-}\mathbf{L}_m)_2](BF_4)_3 + BF_3$$
$$M = Fe(\mathbf{1}),\ Co(\mathbf{2}),\ Cu(\mathbf{4}),\ Zn(\mathbf{5}) \qquad (1)$$

$$2Ni(BF_4)_2 + 2\mathbf{L}_m \xrightarrow{\text{THF}} [Ni_2(\mu\text{-}F)_2(\mu\text{-}\mathbf{L}_m)_2](BF_4)_2(\mathbf{3}) + 2BF_3 \qquad (2)$$

$$2[Cu(CH_3CN)_4]BF_4 + 2\mathbf{L}_m \xrightarrow{\text{THF}} [Cu_2(\mu\text{-}\mathbf{L}_m)_2](BF_4)_2(\mathbf{6}) \qquad (3)$$

The ^1H NMR spectra of **1**−**4** display both the broadened signals and the expanded chemical shift range expected of paramagnetic complexes, and, as a consequence, the observed resonances cannot be assigned with confidence. As reported previously, NMR spectra of the diamagnetic zinc complex **5** indicate the fluoride-bridged dimeric structure remains intact in acetonitrile solution because two distinct, equal intensity environments for the pyrazolyl hydrogen atoms are observed. In addition, the bridging fluoride ligand gives rise to a signal in the ^{19}F NMR spectrum at −211 ppm, and the signal for BF_4^- is found at −150 ppm. In contrast, the Cu(I) complex **6** shows only one set of pyrazolyl ring resonances and in the ^{19}F spectrum only a resonance for the BF_4^- counterion, confirming the lack of a bridging fluoride in this complex. The observation of equivalent pyrazolyl rings for the Cu(I) complex match our earlier data with analogous Ag(I) complexes; both of these d^{10} complexes are expected to be labile.[5b]

Two new experiments were carried out to further characterize the Zn(II) complex in solution. First, a spin saturation ^{19}F NMR experiment shows that irradiation of the resonance at −211 ppm caused no decrease in intensity of the BF_4^- resonance at −150 ppm. Additionally, irradiation at −150 ppm caused no decrease in intensity at the −211 ppm resonance. These results indicate that the bridging fluoride is not exchanging with the BF_4^- on a time scale of about at least minutes.

In addition, to determine the sizes and thus the form of the species in solution, we performed the pulsed−field gradient spin−echo NMR experiment (PGSE−NMR) using both ^1H and ^{19}F.[12] This technique provides an indirect measure of molecular size by the determination of the diffusion coefficient of the complex in solution and has been applied to a number of systems similar to those reported here.[13] Accuracy of the results is believed to be in the 20% range. The experimentally calculated hydrodynamic radius of complex **5** is 6.31 Å from ^1H NMR and 5.93 Å from ^{19}F NMR (on the bridging fluoride); the calculated radius from the solid state structure is 6.44 Å. We also determined the radius of $\mathbf{L}_m$ to be 3.32 Å. The results clearly indicate that the cations of complex **5** remain dimeric in solution. The ligand has a much smaller radius, as expected.

Because of the unusual magnetic properties of the Cu(II) complexes reported herein, vide infra, we have carefully studied the solvation properties of crystals of $\mathbf{4} \cdot 1.5CH_3CN$. This formula of the crystals taken directly from the acetonitrile/Et_2O crystal growth solution and cooled to 150 K on the diffractometer is established by X-ray crystallography. When these crystals are removed from the acetonitrile/Et_2O crystal growth solution, washed with diethyl ether, and allowed to air-dry for 1 h, the crystals still contain acetonitrile as shown by thermogravimetric analysis (TGA) of these crystals that shows the loss of the solvent over the temperature range 25−160 °C. The acetonitrile can also be removed in vacuo without loss of crystallinity. These dried crystals were used for the analytical sample. If allowed to sit a few minutes or weeks in a screw-top vial (filled in air), the crystals pick up water to form $\mathbf{4} \cdot 0.71(H_2O)$ and

(12) (a) Valentini, M.; Pregosin, P. S.; Rüegger, H. *Organometallics* **2000**, *19*, 2551. (b) Stilbs, P. *Prog. NMR Spectrosc.* **1987**, *19*, 1. (c) Hausser, R.; Maier, G.; Noack, F. *Z. Naturforsch.* **1966**, *21a*, 1410.

(13) (a) Moon, K.; Kaifer, A. E. *J. Am. Chem. Soc.* **2004**, *126*, 15016. (b) Reger, D. L.; Gardinier, J. R.; Pellechia, P. J.; Smith, M. D.; Brown, K. J. *Inorg. Chem.* **2003**, *43*, 7635. (c) Reger, D. L.; Elgin, J. D.; Pellechia, P. J.; Smith, M. D.; Simpson, B. K. *Polyhedron* **2009**, *28*, 1469.

Table 2. Important Structural Parameters for $[Fe_2(\mu\text{-}F)(\mu\text{-}\mathbf{L}_m)_2](BF_4)_3\cdot 1.5CH_3CN$ (**1**·1.5CH_3CN), $[Co_2(\mu\text{-}F)(\mu\text{-}\mathbf{L}_m)_2](BF_4)_3\cdot 2.17((CH_3)_2CO)$ (**2**·2.17$((CH_3)_2CO)$), $[Ni_2(\mu\text{-}F)_2(\mu\text{-}\mathbf{L}_m)_2](BF_4)_2\cdot CH_3CN$ (**3**·CH_3CN), $[Cu_2(\mu\text{-}F)(\mu\text{-}\mathbf{L}_m)_2](BF_4)_3\cdot 1.5CH_3CN$ (**4**·1.5CH_3CN), $[Cu_2(\mu\text{-}F)(\mu\text{-}\mathbf{L}_m)_2](BF_4)_3\cdot 2.25((CH_3)_2CO)$ (**4**·2.25$((CH_3)_2CO)$), $[Cu_2(\mu\text{-}F)(\mu\text{-}\mathbf{L}_m)_2](BF_4)_3\cdot 2(H_2O)$ (**4**·2(H_2O)), $[Cu_2(\mu\text{-}F)(\mu\text{-}\mathbf{L}_m)_2](BF_4)_3\cdot 0.71(H_2O)$ (**4**·0.71(H_2O)), and $[Zn_2(\mu\text{-}F)(\mu\text{-}\mathbf{L}_m)_2](BF_4)_3\cdot 1.5CH_3CN$ (**5**·1.5CH_3CN)

complex	metal centers	M−F−M angle, deg	M−F distance, Å	average M−F distance, Å	predicted M−F distance, Å[a]	average M−N distance, Å	M···M distance, Å
1·1.5CH_3CN	Fe(1)--Fe(1′)	180	1.9441(6)	1.96	2.00	2.13	3.89
	Fe(2)--Fe(2′)	177.07(19)	1.9752(6)			2.14	3.95
2·2.17$((CH_3)_2CO)$	Co(1)--Co(1′)	180	1.9521(4)	1.96	1.96	2.09	3.90
	Co(2)--Co(2′)	180	1.9774(4)			2.08	3.96
3·CH_3CN	Ni(1)--Ni(1a)	102.36(10)	2.010(2) F(1) 2.015(2) F(1a)	2.01	1.98	2.12	3.14
4·1.5CH_3CN	Cu(1)--Cu(1′)	164.4(8)	1.93[b]	1.96	1.94	2.06	3.82
	Cu(2)--Cu(2′)	178.50(15)	1.9832(4)			2.07	3.97
4·2.25$((CH_3)_2CO)$	Cu(1)--Cu(1′)	180	1.9194(3)	1.94	1.94	2.05	3.84
	Cu(2)--Cu(2′)	180	1.9574(3)			2.05	3.92
4·2(H_2O)	Cu(1)--Cu(1′)	163.9(8)	1.94[b]	1.96	1.94	2.05	3.83
	Cu(2)--Cu(2′)	173.5(2)	1.9656(5)			2.06	3.93
4·0.71(H_2O)	Cu(1)--Cu(1′)	180	1.9205(7)	1.94	1.94	2.05	3.84
	Cu(2)--Cu(2′)	177.7(3)	1.9621(8)			2.06	3.92
5·1.5CH_3CN	Zn(1)--Zn(1′)	180	1.9385(3)	1.98	1.97	2.10	3.88
	Zn(2)--Zn(2′)	176.61(13)	2.0056(4)			2.11	4.01

[a] Reference 14. [b] Average of the M−F distances due to disorder of the fluoride in the crystal structure.

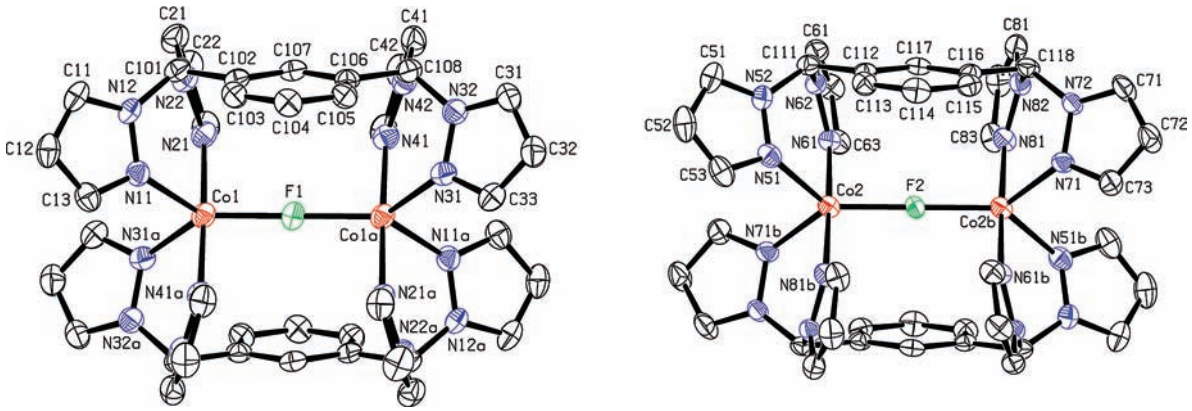

Figure 3. Structures of the two independent cations in $[Co_2(\mu\text{-}F)(\mu\text{-}\mathbf{L}_m)_2](BF_4)_3\cdot 2.17((CH_3)_2CO)$. Hydrogen atoms omitted for clarity.

4·2(H_2O), respectively, as proven by X-ray crystallography. TGA analysis of the **4**·2(H_2O) crystals show the loss of water over the temperature range 25−100 °C.

Solid State Structures. CH_3CN and H_2O Solvates. Figure 2 shows the structures of the two independent cations of $[Cu_2(\mu\text{-}F)(\mu\text{-}\mathbf{L}_m)_2](BF_4)_3\cdot 1.5CH_3CN$ and Table 2 (see Supporting Information, Table S1 for more complete data) shows important bond distances and angles for all five of the new $[M_2(\mu\text{-}F)(\mu\text{-}\mathbf{L}_m)_2](BF_4)_3\cdot$ (CH_3CN or H_2O) complexes. The numbering scheme in Figure 2 is correct for all five structures. The three $[M_2(\mu\text{-}F)(\mu\text{-}\mathbf{L}_m)_2](BF_4)_3\cdot 1.5CH_3CN$ complexes (M = Fe, Cu, Zn) are isostructural, and the structures of the two $[Cu_2(\mu\text{-}F)(\mu\text{-}\mathbf{L}_m)_2](BF_4)_3\cdot x H_2O$ complexes are very similar to them, also in the space group $P2_1/m$. These structures are unusual because one of the two independent complex ions (associated with M(1)) resides on an inversion center whereas the other (associated with M(2)) rests on a plane of symmetry. The unique structural feature is the linear or nearly linear, monobridging fluoride ligand. In two of the structures, **4**·1.5CH_3CN and **4**·2(H_2O), the crystallographic data for the centrosymmetric copper site was best modeled as having two equally populated sites with bent Cu−F−Cu angles (Figure 2, left). The crystallographic solution with a linear Cu−F−Cu bond angle had about the same *R* values, but the fluoride ellipsoid was elongated.

In all of these structures, the geometries about the metal cations are trigonal bipyramidal with equatorially bonded atoms N(11, 71), N(31a, 51), and F(1, 2) and axially bonded N(21, 81) and N(41a, 61) for M(1, 2), respectively. The largest distortion from this structural arrangement is in the equatorial planes in the N(11)−M(1)−N(31a) and N(51)−M(2)−N(71) angles that average 95.5° and 92.2°, respectively.

Acetone Solvates. The cationic structure for $[Co_2(\mu\text{-}F)(\mu\text{-}\mathbf{L}_m)_2](BF_4)_3\cdot 2.17((CH_3)_2CO)$ is isostructural to $[Cu_2(\mu\text{-}F)(\mu\text{-}\mathbf{L}_m)_2](BF_4)_3\cdot 2.25((CH_3)_2CO)$. The structure of the cation in **2**·2.17$((CH_3)_2CO)$ is shown in Figure 3, same numbering for **4**·2.25$((CH_3)_2CO)$), and Table 2 (see Supporting Information, Table S2 for more complete information) gives important bond distances and angles for both. The structures of the cations in these two complexes are very similar to the structures of $[M_2(\mu\text{-}F)(\mu\text{-}\mathbf{L}_m)_2](BF_4)_3\cdot$($CH_3CN$ or H_2O), with each metal ion in a trigonal bipyramidal coordination environment. In these two structures, the two independent cationic units each lie on crystallographic inversion centers coincident with the bridging fluoride atoms.

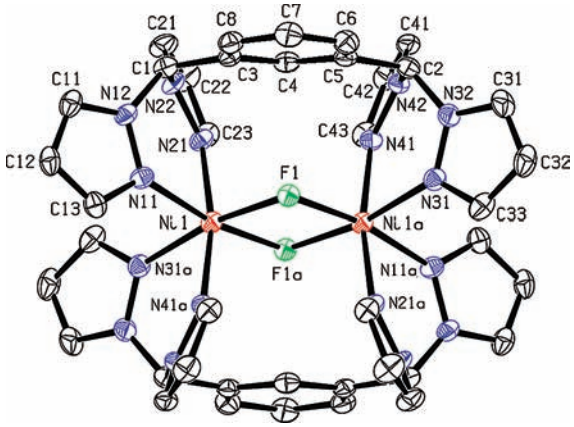

Figure 4. Structure of the cation in $[Ni_2(\mu\text{-}F)_2(\mu\text{-}\mathbf{L}_m)_2](BF_4)_2 \cdot CH_3CN$. The hydrogen atoms have been omitted for clarity.

As shown in Table 2, the M−F distances for a given metal are different in the two crystallographic sites for each complex. For the three isostructural $[M_2(\mu\text{-}F)(\mu\text{-}\mathbf{L}_m)_2](BF_4)_3 \cdot 1.5CH_3CN$ (M = Fe, Cu, Zn) complexes, where M(1) sits on an inversion center and M(2) on a mirror plane, the difference in M−F distances are large (Fe(II) 0.03 Å, Cu(II) 0.05 Å, and Zn(II) 0.07 Å) and always in the same direction, with the M(1)-F distances always shorter. For the bridging fluoride in two of the Cu(II) structures, $\mathbf{4} \cdot 1.5CH_3CN$ and $\mathbf{4} \cdot 2(H_2O)$, where the crystallographic data for the centrosymmetric site was best modeled as having two equally populated sites with a bent Cu−F−Cu, this disorder had little effect on the overall metrics of the structures. The two $[M_2(\mu\text{-}F)(\mu\text{-}\mathbf{L}_m)_2](BF_4)_3 \cdot x(CH_3)_2CO$ (M = Co(II), Cu(II)) structures also have two independent sites that show different M−F distances, but in these cases both metal sites are on a center of symmetry. For all four forms of **4** the average M−F distance is about the same and close to the value predicted by the sum of the ionic radii of the Cu(II) and fluoride.[14]

Dibridged Nickel Complex. The structure of the cation in $\mathbf{3} \cdot CH_3CN$ is shown in Figure 4, and important bond distances and angles are shown in Table 2 (see Supporting Information, Table S3 for more complete information). This nickel containing complex has two bridging fluoride ligands, unlike the other first row metal complexes reported herein. Each Ni(II) ion resides in a distorted octahedral environment, where the angles between atoms at opposite apexes of the octahedra are less than 180° with angles of 170°, 169°, and 170°. We have reported a difluoride bridged cadmium complex, which also has a distorted octahedral environment around the metal center.[5c] The bent Ni−F═Ni angles result in a significant metal···metal distance decrease when compared to a single, linear or nearly linear fluoride bridge. The single, linear or nearly linear fluoride bridge metal···metal distances range from 3.82 Å to 4.01 Å, but the nickel···nickel nonbonding distance is much shorter at 3.14 Å.

Magnetic Properties. As would be expected from the structures of **1**−**4**, these dimeric complexes are magnetically dilute and, except for **4**, exhibit paramagnetic behavior at higher temperatures and show weak intramolecular antiferromagnetic exchange coupling and zero-field splitting at lower temperatures; there is no evidence for any long-range magnetic order in any of the complexes reported here.

The temperature dependence of the molar magnetic susceptibility, χ_M, and $1/\chi_M$ of **1** is shown in Supporting Information, Figure S1, and of $\chi_M T$ and $1/\chi_M$ is shown in Figure 5. As is shown in the inset to Figure 5, $1/\chi_M$ is linear and obeys the Curie−Weiss law above 135 K; a linear fit yields a Weiss temperature, θ, of −99 K, a Curie constant, C, of 7.09 emu K/mol, and a corresponding effective magnetic moment, μ_{eff}, of 7.53 μ_B/mol of dimer or 5.32 μ_B/mol Fe; the latter moment is typical of high-spin iron(II) with $S = 2$ and $g = 2.17$; a g-value slightly above 2 indicates that there is at most only a relatively small influence of spin−orbit coupling upon the magnetic properties of **1**.

Below 135 K, χ_M of **1** deviates from Curie−Weiss behavior and exhibits a maximum at about 75 K, see Supporting Information, Figure S1, as a result of intramolecular antiferromagnetic exchange coupling between the two iron(II) ions and the associated depopulation of the higher-value S states and the increasing population of the smaller-value S states as the temperature decreases. As is shown in Figure 5, the observed $\chi_M T$, measured between 2 and 300 K, can be fit[15] with the following Hamiltonian,

$$\mathscr{H} = -2JS_1 \cdot S_2 + D_1 S_{z,1}{}^2 + E_1(S_{x,1}{}^2 + S_{y,1}{}^2) + D_2 S_{z,2}{}^2 + E_2(S_{x,2}{}^2 + S_{y,2}{}^2)$$

with $g = 2.12(2)$ or $2.15(2)$, an antiferromagnetic exchange coupling constant, J, of $-10.4(2)$ cm^{-1}, and zero-field splitting parameters, D and E, of $-10.2(3)$ and $-2.0(5)$ cm^{-1}, respectively, values that are expected for both the distorted five-coordinate iron(II) environment of **1** and the fluoride bridge between two high-spin iron(II) ions. The full details of the use of this Hamiltonian in the fit are given in the Supporting Information. At this point it should be noted that the 150 K crystal structure[5c] of **1** reveals two chemically very similar, but crystallographically independent, iron(II) dimers. Thus, the above parameters are actually the average for the two iron(II) dimers. One of the dimers has a linear bridge with Fe(1)−F(1) bond distances of 1.9441(6) Å and an Fe(1)−F(1)−Fe(1a) bond angle of 180°, whereas the second dimer has a non-linear bridge with Fe(2)−F(2) bond distances of 1.9752(6) Å and an Fe(2)−F(2)−Fe(2a) bond angle of 177.07(19)°; in neither dimer is there axial symmetry about the Fe−F−Fe bridge. Thus, the observed average E-value of $-2.0(5)$ cm^{-1} may be a bit larger than expected but is feasible in view of the non-axial average structures of the two crystallographically distinct iron(II) dimers. The misfit observed in the fits shown in Figure 5 above about 150 K probably indicates that J changes slightly with increasing temperature as a result of small structural changes in the fluoride bridging angle of **1** upon warming.

(14) Shannon, R. D. *Acta Crystallogr.* **1976**, *A32*, 751; Note, while the ionic radius of high spin Fe(II) in a 5-coordinate environment is not given in the table, a value of 0.85 Å can be calculated from both the extrapolation of the differences in values given for 4-coordination or from the average M−N bond distances of these complexes taking into account the known metal radii of Co(II), Cu(II), and Zn(II).

(15) Borràs-Almenar, J. J.; Clemente-Juan, J. M.; Coronado, E.; Tsukerblat, B. S. *J. Comput. Chem.* **2001**, *22*, 985.

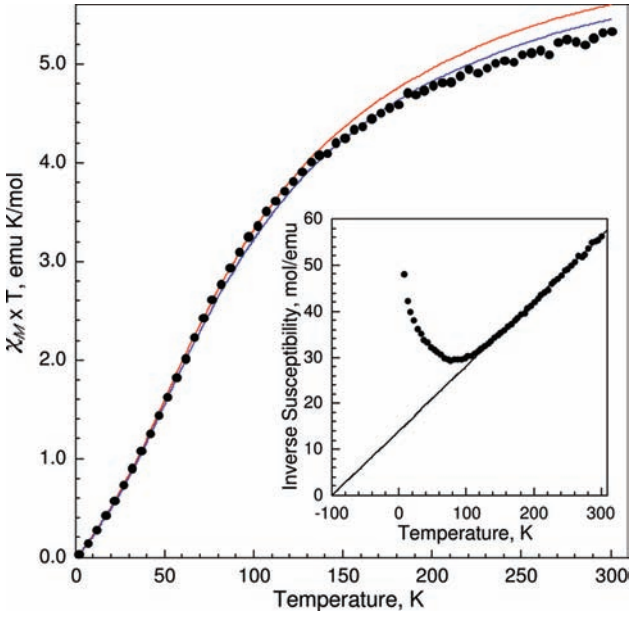

Figure 5. Temperature dependence of $\chi_M T$ of **1**, where the fit corresponds to $S = 2$, $J = -10.4(2)$ cm^{-1}, $D = -10.2(3)$ cm^{-1}, and $E = -2.0(5)$ cm^{-1}, and $g = 2.12(2)$ for the blue line and $g = 2.15(2)$ for the red line. Inset: The temperature dependence of $1/\chi_M$ and a Curie−Weiss law linear fit from 135 to 300 K.

The temperature dependence of $\chi_M T$ and $1/\chi_M$ of **2** is shown in Figure 6 and its inset. As is shown in the inset, $1/\chi_M$ is linear and obeys the Curie−Weiss law above 40 K; a linear fit yields a θ of −16 K, a C of 5.91 emu K/mol of dimer, and a corresponding μ_{eff} of 6.87 μ_B/mol dimer and 4.86 μ_B/mol Co. The latter moment is somewhat higher than expected for a high-spin cobalt(II) complex with $S = 3/2$ and $g = 2$; the corresponding g-value is 2.51, indicating the potential significance of spin−orbit coupling in determining the magnetic properties of **2**.

Below 40 K, $1/\chi_M$ of **2** deviates from Curie−Weiss behavior predominately as a result of a combination of spin−orbit coupling and zero-field splitting; a fit[15,16] of $\chi_M T$ between 5 and 300 K with $S = 3/2$ yields $g = 2.45(1)$, $zJ = -0.67(5)$ cm^{-1}, $|D| = 61(2)$ cm^{-1}, and a temperature independent paramagnetic contribution, $N\alpha$, of 0.00031 emu/mol. The rather large magnitude of the D-value is not unexpected for a distorted high-spin cobalt(II) complex.[17] The full details and expressions used in the fit are given in the Supporting Information.

There have been relatively few reports of the zero-field splitting of cobalt(II) complexes and, to the best of our knowledge, no such reports for five-coordinate cobalt(II). However, Marshall, et al. have reported[16c] a value of $|D| = 38.9$ cm^{-1} in a complex containing pseudooctahedral cobalt(II), Lohr, et al. have reported[17] a value of 87.2 cm^{-1} for a highly tetragonally distorted pseudooctahedral cobalt(II) complex, and Makinen, et al. have found[18] a value of 53 cm^{-1} for [Co(pyridine-*N*-oxide)$_6$](ClO$_4$)$_2$, a

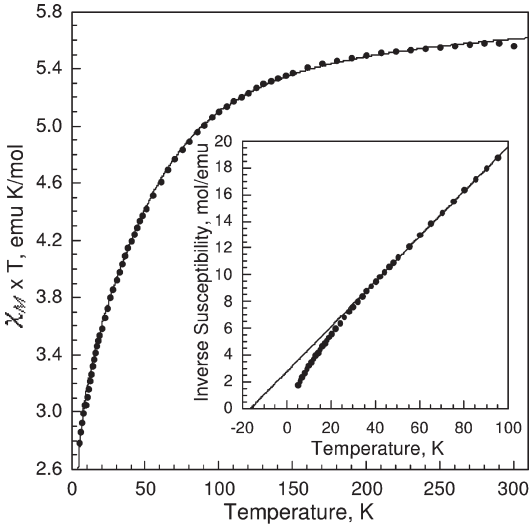

Figure 6. Temperature dependence of χ_MT of **2**, where the solid line corresponds to a fit with $S = 3/2$, $g = 2.45(1)$, $zJ = -0.67(5)$ cm^{-1}, $|D| = 61(2)$ cm^{-1}, and $N\alpha = 0.00031$ emu/mol. Inset: The temperature dependence of $1/\chi_M$ and a Curie−Weiss linear fit from 40 to 300 K.

complex with at most a very small trigonal distortion from cobalt(II) octahedral coordination geometry. In contrast, Duran, et al. have reported[19] a value of $D = 10.8(2)$ cm^{-1} for a pseudotetrahedral cobalt(II) complex. Thus it seems that the value of $|D| = 61(2)$ cm^{-1} observed for **2**, which has a distorted five-coordinate coordination environment, is not unusual.

The temperature dependence of $\chi_M T$ and $1/\chi_M$ of **3** is shown in Figure 7 and its inset. As is shown in this inset, $1/\chi_M$ is linear and obeys the Curie−Weiss law between 5 and 300 K; a linear fit yields a θ of −0.45 K, a C of 2.06 emu K/mol, and a corresponding μ_{eff} of 4.06 μ_B/mol of dimer or 2.87 μ_B/mol Ni; the latter moment is slightly higher than expected for a nickel(II) complex with $S = 1$ and the observed moment indicates that $g = 2.029$. A fit of $\chi_M T$ between 5 and 300 K obtained by using the method of Ginsberg and co-workers[20] and $S = 1$ yields $g = 2.030(1)$, $J = -0.214(6)$ cm^{-1}, and $D = -3.0(1)$ cm^{-1}, values that are reasonable in view of the difluoro-bridged structure of **3**.

The magnetic properties of three different solvates of **4** are very different from **1**−**3** and, surprisingly, correspond to a diamagnetic complex of copper(II), see Figure 8. After applying a diamagnetic correction of −0.000605 emu/mol of dimer, the diamagnetic χ_M of **4** is −0.00050(1) emu/mol of dimer at 300 K and is virtually independent of temperature between 5 and 400 K, a result that has been confirmed through two separate preparations and three separate magnetic studies. The very small negative χ_M value implies that the diamagnetic correction may be in error by this amount; there is no indication of any second order Zeeman contribution to χ_M in **4**. The absence of any paramagnetic moment between 5 and 400 K indicates that, if $S = 1/2$ and $g = 2$, J would be at least −600 cm^{-1} or even more negative.

(16) (a) O'Connor, C. J. *Prog. Inorg. Chem.* **1982**, *29*, 203. (b) Miyasaka, H.; Clérac, R.; Campos-Fernández, C. S.; Dunbar, K. R. *Inorg. Chem.* **2001**, *40*, 1663. (c) Marshall, S. R.; Rheingold, A. L.; Dawe, L. N.; Shum, W. W.; Kitamura, C.; Miller, J. S. *Inorg. Chem.* **2002**, *41*, 3599.

(17) Lohr, L. L.; Miller, J. C.; Sharp, R. R. *J. Chem. Phys.* **1999**, *111*, 10148.

(18) Makinen, M. W.; Kuo, L. C.; Yim, M. B.; Wells, G. B.; Fukuyama, J. M.; Kim, J. E. *J. Am. Chem. Soc.* **1985**, *107*, 5245.

(19) Duran, N.; Clegg, W.; Cucurull-Sánchez, L.; Coxall, R. A.; Jiménez, H. R.; Moratal, J.-M.; Lloret, F.; González-Duarte, P. *Inorg. Chem.* **2000**, *39*, 4821.

(20) (a) Ginsberg, A. P. *Inorg. Chim. Acta* **1971**, *5*, 45. (b) Ginsberg, A. P.; Martin, R. L.; Brooks, R. W.; Sherwood, R. C. *Inorg. Chem.* **1972**, *11*, 2884.

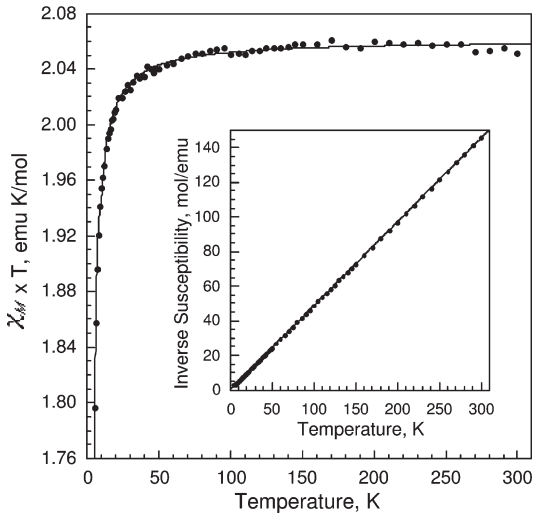

Figure 7. Temperature dependence of $\chi_M T$ of **3**. The solid line corresponds to a fit with $S = 1$, $g = 2.030(1)$, $J = -0.214(6)$ cm^{-1}, and $D = -3.0(1)$ cm^{-1}. Inset: The temperature dependence of $1/\chi_M$ and a Curie−Weiss linear fit from 5 to 300 K.

Confirmation of the Oxidation State of $[Cu_2(\mu\text{-}F)(\mu\text{-}L_m)_2](BF_4)_3$, 4. An alternative possibility for the unexpected diamagnetic properties of the three solvates of **4** is that the complexes could actually contain Cu(I) ions, ions that would be expected to be diamagnetic. However, this possibility has been eliminated on the basis of the following studies. The initial formula of the Cu(II) dimer isolated in crystalline form is **4**·1.5CH_3CN, the form of the sample obtained when the crystals are quickly removed from the crystal growth solution. When this sample is collected, washed with diethyl ether, and allowed to air-dry for 1 h, the acetonitrile is still present, but can be removed in vacuo without loss of crystallinity. As described above, these dried crystals absorb water from the air to form **4**·0.71(H_2O) and **4**·2(H_2O). We have carried out magnetic studies, on all three of these forms of the dimer, and all show results identical to those shown in Figure 8 for **4**·0.71(H_2O). Following each of the magnetic studies, the crystals used underwent an X-ray crystallographic analysis and were found to be the three different forms of the Cu(II) dimer characterized crystallographically above. Thus, we have crystallographic evidence that the three samples used in the magnetic studies contain Cu(II) ions.

Additional support for Cu(II) ions in **4** comes from the reaction of the Cu(I) complex $[Cu(CH_3CN)_4]BF_4$ with $\mathbf{L}_m$ to yield $[Cu_2(\mu\text{-}\mathbf{L}_m)_2](BF_4)_2$, **6**, the Cu(I) analogue of the previously reported Ag(I) complexes.[5b] Although we have been unable to grow single crystals of **6**, NMR, mass spectrometry, and elemental analyses clearly indicate its formulation as a binuclear Cu(I) complex. Further, as expected for a d^{10} Cu(I) ion, the complex is white, and the reflectance spectrum of **6** exhibits no reflectance bands between 375 and 800 nm. In contrast, the Cu(II) samples used in the above magnetic studies are blue and exhibit a reflectance band at 486 nm. Also, the mass spectra of the two complexes are clearly different. In the case of **4** the mass spectra show peaks associated with Cu(II) species, most notably $[Cu_2(\mathbf{L}_m)_2F]^{3+}$ and, in the case of **6**, the $[Cu_2(\mathbf{L}_m)_2BF_4]^+$ peak for Cu(I).

Finally, we have measured the solid state ^{13}C NMR spectra of both **4** and **6**. The spectrum of **6** shows several resonances that correspond to aromatic carbon atoms: two broad resonances around 140 ppm, a single broad resonance at 132 ppm, multiple resonances centered around 125 ppm, a single broad resonance at 106 ppm, and a single resonance corresponding to the methine carbon at 74 ppm. This complex spectrum was expected based on the crystallographic study of the analogous Ag(I) complex[5b] that shows the pyrazolyl rings as existing in at least two distinct environments. In contrast, the spectrum of **4** has a single resonance at 137 ppm, and multiple broad resonances at about 132 ppm. Thus, a comparison of the two spectra shows that several resonances in **6** have been suppressed in **4**, such as the broad resonance at about 140 ppm, the resonance at 106 ppm, and the methine carbon resonance at 74 ppm. Observation of some resonances for carbon in the ligand backbone of **4** supports the diamagnetic nature of **4** in the solid state. We propose that the pyrazolyl resonances are the ones not observed in this spectrum of **4** and a possible explanation for the loss of many resonances is the impact of a very low population of the triplet state causing line broadening of the resonances of carbon atoms located closer to the Cu(II) ion. We note that under similar conditions no spectrum was observed for the fully paramagnetic iron(II) complex, **1**

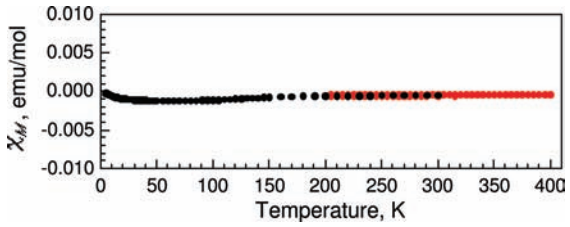

Figure 8. Diamagnetic behavior of **4**·0.71H_2O, black dots 5−300 K, red dots 200−400 K.

Mössbauer Spectral Properties. The Mössbauer spectra of **1** have been measured from 4.2 to 295 K and fit with a symmetric quadrupole doublet; some of the spectra are shown in Figure 9 and the resulting spectral parameters are given in Table 3 and shown in part in Figure 10. The observed spectra indicate that, as expected, **1** exhibits no long-range magnetic order between 4.2 and 295 K; however, the spectra are fully consistent with the presence of intramolecular antiferromagnetic exchange below 135 K.

The observed isomer shifts are completely consistent with the presence of five-coordinate high-spin iron(II). The temperature dependence of the isomer shift of **1**, see the top of Figure 10, is well fit with the Debye model[21] for the second-order Doppler shift with a characteristic Mössbauer temperature, Θ_M, of 530(30) K, a value that is reasonable for a five-coordinate iron(II) ion bonded to a fluoride ion.

The temperature dependence of the logarithm of the Mössbauer spectral absorption area of **1**, see the bottom of Figure 10, is also well fit with the Debye model[21] for a solid and yields a Debye temperature, Θ_D, of 129(3) K, a value that is substantially smaller than the

(21) Shenoy, G. K.; Wagner, F. E.; Kalvius, G. M. In *Mössbauer Isomer Shifts*; Shenoy, G. K., Wagner, F. E., Eds.; North-Holland: Amsterdam, 1978; p 49.

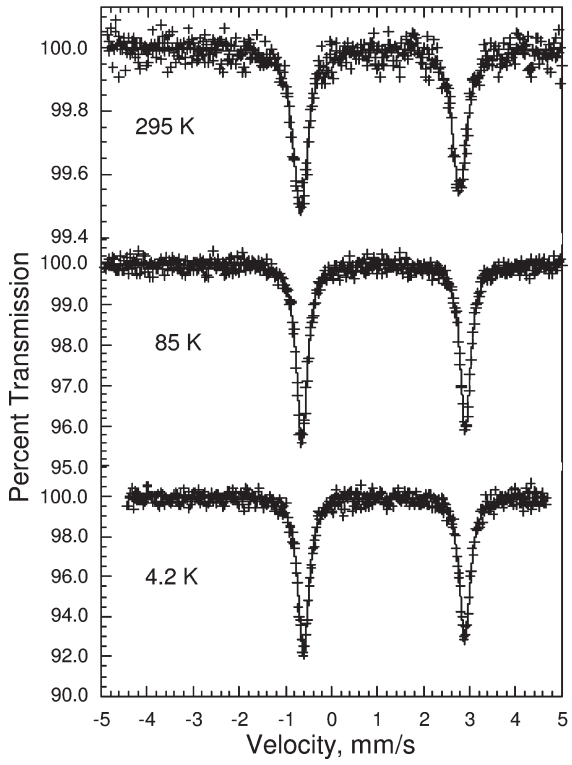

Figure 9. Mössbauer spectra of **1** obtained at the indicated temperatures.

Table 3. Mössbauer Spectral Parameters of **1**

T, K	δ, mm/s[a]	ΔE_Q, mm/s	Γ, mm/s	absolute area, (%ε)/(mm/s)
295	1.047	3.46	0.37	0.551
225	1.080	3.50	0.38	1.272
155	1.109	3.53	0.29	2.236
85	1.138	3.55	0.28	3.605
65	1.140	3.56	0.28	4.057
45	1.146	3.57	0.30	4.771
25	1.149	3.565	0.29	5.116
4.2	1.147	3.565	0.29	5.109

[a] The isomer shifts are given relative to 295 K α-iron powder.

Θ_M value of 530(30) K. It is well-known[21] that the two temperatures, Θ_M and Θ_D, obtained from the two temperature dependencies, are usually different because they depend on $\langle v^2 \rangle$ and $\langle x^2 \rangle$, respectively, where $\langle v^2 \rangle$ is the root-mean-square vibrational velocity of the iron-57 nuclide and $\langle x^2 \rangle$ is the root-mean-square displacement of the iron-57 nuclide; unfortunately, there is no model independent relationship[21] between these mean-square values. However, the values of these temperatures reported[22] for other iron(II) complexes indicate that Θ_M, which is more sensitive to the high-frequency phonons, is often two to four times larger than Θ_D.

The temperature dependence of the quadrupole splitting, ΔE_Q, is shown in the center of Figure 10. It should be noted that the 0.10 mm/s or 2.9% decrease in ΔE_Q is very small; an attempt to fit the temperature dependence of ΔE_Q with the Ingalls' model[23] failed because of this small change. Alternatively, the solid line in Figure 10 is the result of a fit with the equation

$$\Delta E_Q(T) = \Delta E_Q(0)[1 - aT - bT^2] \qquad (4)$$

with ΔE_Q (0) = 3.565 mm/s, $a = 1.2 \times 10^{-5}$ K^{-1}, and $b = 3.02 \times 10^{-7}$ K^{-2}.

The high-spin iron(II) quadrupole splitting consists of two contributions, a valence contribution and a lattice contribution. The valence contribution arises from the low-symmetry splitting of the ground state t_{2g} orbitals of iron(II) by the rhombic crystal field, a splitting that must be large enough that, between 4.2 and 300 K, the thermal population of the first excited state orbital or orbitals is virtually zero, that is, the first excited state orbital must be approximately 1000 cm^{-1} above the ground state orbital and be populated at all temperatures with only one electron. In this case there will be no temperature dependence of the valence contribution to ΔE_Q and the Ingalls' model does not apply. In contrast, the lattice contribution to ΔE_Q, which usually subtracts from the valence contribution, is weakly temperature dependent because of lattice

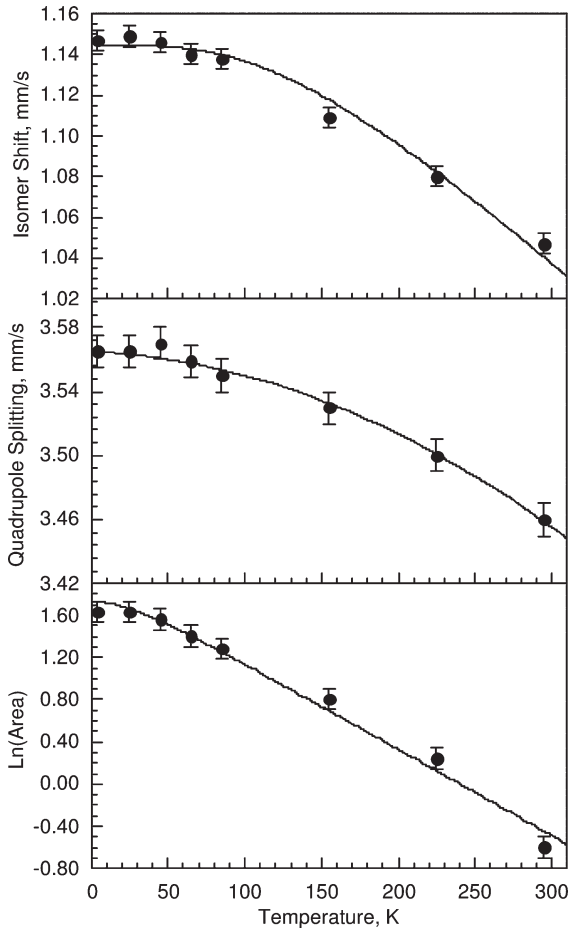

Figure 10. Temperature dependence of the Mössbauer spectral isomer shifts, quadrupole splittings, and the logarithm of the spectral absorption areas of **1**. The lines through the isomer shifts and the logarithm of the spectral absorption areas correspond to fits with the Debye model for a solid. The line through the quadrupole splitting corresponds to a fit with eq 4; the reason for the very small change in the quadrupole splitting with temperature is discussed in the text.

(22) Owen, T.; Grandjean, F.; Long, G. J.; Domasevitch, K. V.; Gerasimchuk, N. *Inorg. Chem.* **2008**, *47*, 8704, and the references given therein.
(23) Ingalls, R. *Phys. Rev. A* **1964**, *133*, 787.

expansion upon warming. The small *a* and *b* parameters obtained from the quadratic fit given above agree well with those expected for a typical lattice expansion.

Discussion

Our initial work with Ag(I) chemistry indicated that the ditopic ligand $\mathbf{L}_m$ supported bimetallic complexes as shown in Figure 1a. In contrast, with more highly charged Fe(II), Co(II), Cu(II), and Zn(II) ions, the bimetallic complexes abstract fluoride ion from the BF_4^- counterion to form the monobridged $[M_2(\mu\text{-F})(\mu\text{-}\mathbf{L}_m)_2](BF_4)_3$ complexes. The higher charge and preferred higher coordination numbers of these metal ions are critical for this chemistry because like Ag(I), reaction of $\mathbf{L}_m$ with $[Cu(CH_3CN)_4]BF_4$ also forms the nonbridged dimeric $[Cu_2(\mu\text{-}\mathbf{L}_m)_2](BF_4)_2$ complex.

The most interesting structural feature of all seven of the monobridged complexes is the linear, or very nearly linear, bridged M−F−M bonding. NMR studies on solutions of $[Zn_2(\mu\text{-F})(\mu\text{-}\mathbf{L}_m)_2](BF_4)_3$ show this dimeric, fluoride bridged structure is retained in solution. To the best of our knowledge, only one such linear M−F−M arrangement in discrete dimeric complexes existed prior to our studies, a zinc(II) bimetallic complex bonded to a ligand containing a *meta*-substituted pyridine with bis(imidazolyl)methylene donor groups.[7h] A nearly linear 175.6 °Fe−F−Fe bond angle has been reported in a tetranuclear iron(III) species.[24] While many bimetallic bridging complexes do exist, they are generally dibridged with, of course, bent M−F−M angles.[6,25] A number of monobridged, bent M−F−M complexes have also been reported.[26] Interestingly, with Ni(II), the dibridged $[Ni_2(\mu\text{-F})_2(\mu\text{-}\mathbf{L}_m)_2](BF_4)_2$ complex is isolated from reactions that are similar to those used to prepare the other divalent first row transition metal complexes. The reasons for the formation of this different complex with Ni(II) are not clear.

With the exception of Fe(II), the M−F distances in all the structures are close to the predicted values,[14] see Table 2. In the case of Fe(II), which has the largest ionic radius, the observed distance is 0.04 Å shorter than predicted. This metric, and the accompanying metal ion···metal ion distances that range from 3.82 to 4.01 Å, is likely influenced by the $\mu\text{-}\mathbf{L}_m$ ligands, but clearly shows that the M−F bond distances are as expected for "normal" M−F bonding.

The M−F distances and the accompanying M−F−M angles are important because they influence intramolecular magnetic exchange interactions. It has been noted[25e] that intramolecular antiferromagnetic exchange interactions should be at a maximum in a bimetallic complex with a single bridging monoanionic ligand, *X*, when the M−*X*−M angle is 180°. The main conclusion of the magnetic studies, as summarized in Table 4, is that the number of metal ion 3d electrons has a strong influence on the antiferromagnetic exchange coupling. Both **1**, the iron(II) complex, and **2**, the cobalt(II) complex, have surprisingly small intramolecular antiferromagnetic exchange coupling constants, *J*, of −10.4(2) and −0.20(5) cm^{-1}, respectively. The deviations from Curie−Weiss behavior as a consequence of this exchange are only apparent below 135 and 40 K, respectively, see the insets to Figures 5 and 6. In contrast, three different solvates of **4**, the copper(II) complex, are fully diamagnetic between 5 and 400 K with a *J* value that must be more negative than −600 cm^{-1}. These results apparently represent the first report of a *large* difference in the intramolecular antiferromagnetic exchange behavior of a $3d^9$ metal ion as compared with the $3d^6$ and $3d^7$ metal ions in a monobridged, binuclear complex. The number of 3d metal ion electrons must be the key issue because the iron(II) complex has the shortest M−F distance as compared to the predicted values. Further, the M−F distance in all three of the complexes is nearly the same, with an average range of only 1.94 to 1.96 Å.

Table 4. Solid State Magnetic Properties

Complex	*J*, cm^{-1}	*g*	*D*, cm^{-1}	*E*, cm^{-1}
$[Fe_2(\mu\text{-F})(\mu\text{-}\mathbf{L}_m)_2](BF_4)_3$, **1**	−10.4(2)	2.12(2) to 2.15(2)	−10.2(3)	−2.0(5)
$[Co_2(\mu\text{-F})(\mu\text{-}\mathbf{L}_m)_2](BF_4)_3$, **2**	−0.67(5)	2.45(1)	±61(2)	
$[Cu_2(\mu\text{-F})(\mu\text{-}\mathbf{L}_m)_2](BF_4)_3$, **4**	< −600			

Hoffmann and co-workers[27] have investigated the bonding and accompanying magnetic effects for the Cu(II)−*X*−Cu(II), $3d^9$ electronic configuration in a number of geometries including the trigonal bipyramidal geometry observed herein, using $[Cl_4CuClCuCl_4]^{5-}$ as the model compound. The highest occupied molecular orbital (HOMO) is a sideways symmetric antibonding combination of $3d_{z^2}$ type orbitals interacting with the Cl 3s orbital and the lowest unoccupied molecular orbital (LUMO) is the antisymmetric combination of the same metal orbitals interacting with a Cl 3p orbital, see Figure 11. The calculations show a substantial separation in these two orbitals, that is, a substantial HOMO−LUMO gap, a gap that supports antiferromagnetic exchange interactions. One known example of a Cu(II)−Cl−Cu(II) complex of this type has $J = -144$ cm^{-1}.[28] As outlined in these calculation, elsewhere,[25e] and in density functional calculations on dibridged, octahedral, Cu(II) complexes,[29] antiferromagnetic coupling should be larger for a bridging fluoride, where the bridging orbitals are the 2s and 2p orbitals of the fluoride ion, than for the chloride ion. Given the presence of the linear, or nearly linear, bridging fluoride in the four Cu(II) complexes reported herein, intramolecular antiferromagnetic exchange coupling should be expected to be large, making our *unusual J* of more negative than −600 cm^{-1} for **4** somewhat anticipated, but only, as observed, for the complexes **4** that contain Cu(II) $3d^9$ ions. Additional theoretical and experimental work is required to better understand the

(24) Westerheide, L.; Müller, F. K.; Than, R.; Krebs, B.; Dietrich, J.; Schindler, S. *Inorg. Chem.* **2001**, *40*, 1951.

(25) (a) Reitmeijer, F. J.; de Graaff, R. A. G.; Reedijk, J. *Inorg. Chem.* **1984**, *23*, 151. (b) Lee, S. C.; Holm, R. H. *Inorg. Chem.* **1993**, *32*, 4745. (c) Casellas, H.; Pevec, A.; Kozlevčar, B.; Gamez, P.; Reedijk, J. *Polyhedron* **2005**, *24*, 1549. (d) Jacobson, R. R.; Tyeklár, Z.; Karlin, K. D.; Zubieta, J. *Inorg. Chem.* **1991**, *30*, 2035. (e) Brezinski, M. M.; Schneider, J.; Radonovich, L. J.; Klabunde, K. J. *Inorg. Chem.* **1989**, *28*, 2414. (f) Velthuizen, W. C.; Haasnoot, J. G.; Kinneging, A. J.; Rietmeijer, F. J.; Reedijk, J. *J. Chem. Soc., Chem. Commun.* **1983**, 1366. (e) Rietmeijer, F. J.; van Albada, G. A.; de Graaff, R. A. G.; Haasnoot, J. G.; Reedijk, J. *Inorg. Chem.* **1985**, *24*, 3597.

(26) (a) Emsley, J.; Arif, M. *J. Chem. Soc., Dalton Trans.* **1989**, 1273. (b) Meyer, F.; Heinze, K.; Nuber, B.; Zsolnai, L. *J. Chem. Soc., Dalton Trans.* **1998**, 207. (c) Blake, A. J.; Devillanova, F. A.; Garau, A.; Harrison, A.; Isaia, F.; Lippolis, V.; Tiwary, S. K.; Schröder, M.; Verani, G.; Whittaker, G. *J. Chem. Soc.; Dalton Trans.* **2002**, 4389. (d) Rietmeijer, F. J.; Haasnoot, J. G.; den Hartog, A. J.; Reedijk, J. *Inorg. Chim. Acta* **1986**, *113*, 147.

(27) Hay, J. P.; Thibeault, J. C.; Hoffmann, R. *J. Am. Chem. Soc.* **1975**, *97*, 4884.

(28) Duggan, D. M.; Jungst, R. G.; Mann, K. R.; Stucky, G. D.; Hendrickson, D. N. *J. Am. Chem. Soc.* **1974**, *96*, 3443.

(29) Rodriguez-Fortea, A.; Alemany, P.; Alvarez, S.; Ruiz, E. *Inorg. Chem.* **2002**, *41*, 3769.

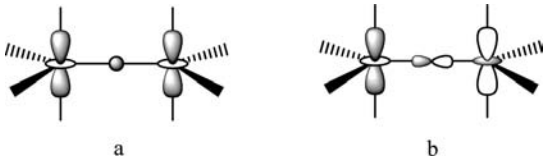

Figure 11. Antibonding combination of d_{z^2} type orbitals interacting with (a) the s-orbital to give the HOMO sideways symmetric combination or (b) the p-orbital to give the LUMO antisymmetric combination.

trends reported herein for the Fe(II) and Co(II) complexes. In contrast, in the Ni(II), dibridged complex **3** the antiferromagnetic exchange coupling through bridging groups at 102° is expected and observed to be very weak.

Acknowledgment. The authors acknowledge the National Science Foundation (CHE-0715559) and the Fonds National de la Recherche Scientifique, Belgium (Grants 9.456595 and 1.5.064.05) for financial support. We thank Dr. William Cotham for obtaining the mass spectrometry data and the reviewers for helpful discussions on the magnetic properties.

Supporting Information Available: Tables on bond distances and angles, methods and equations used for the magnetic fits and temperature dependence of the molar magnetic susceptibility of **1**. X-ray crystallographic files in CIF format and details of the fitting of the magnetic data. This material is available free of charge via the Internet at http://pubs.acs.org.